Chin. Phys. B Vol. 30, No. 12 (2021) 127402

SPECIAL TOPIC — Unconventional superconductivity

Dispersion of neutron spin resonance mode in $Ba_{0.67}K_{0.33}Fe_2As_2$*

Tao Xie(谢涛)[1,2,†§], Chang Liu(刘畅)[1,2,†], Tom Fennell[3], Uwe Stuhr[3],
Shi-Liang Li(李世亮)[1,2,4], and Hui-Qian Luo(罗会仟)[1,4,‡]

[1] *Beijing National Laboratory for Condensed Matter Physics, Institute of Physics, Chinese Academy of Sciences, Beijing* 100190, *China*
[2] *School of Physical Sciences, University of Chinese Academy of Sciences, Beijing* 100190, *China*
[3] *Laboratory for Neutron Scattering and Imaging, Paul Scherrer Institut, CH-5232 Villigen PSI, Switzerland*
[4] *Songshan Lake Materials Laboratory, Dongguan* 523808, *China*

(Received 22 September 2021; revised manuscript received 1 November 2021; accepted manuscript online 4 November 2021)

We report an inelastic neutron scattering investigation on the spin resonance mode in the optimally hole-doped iron-based superconductor $Ba_{0.67}K_{0.33}Fe_2As_2$ with $T_c = 38.2$ K. Although the resonance is nearly two-dimensional with peak energy $E_R \approx 14$ meV, it splits into two incommensurate peaks along the longitudinal direction ($[H,0,0]$) and shows an upward dispersion persisting to 26 meV. Such dispersion breaks through the limit of total superconducting gaps $\Delta_{tot} = |\Delta_k| + |\Delta_{k+Q}|$ (about 11–17 meV) on nested Fermi surfaces measured by high resolution angle resolved photoemission spectroscopy (ARPES). These results cannot be fully understood by the magnetic exciton scenario under $s^{\pm}$-pairing symmetry of superconductivity, and suggest that the spin resonance may not be restricted by the superconducting gaps in the multi-band systems.

Keywords: iron-based superconductor, neutron spin resonance, magnetic excitations

PACS: 74.70.Xa, 75.30.Gw, 78.70.Nx **DOI:** 10.1088/1674-1056/ac3651

1. Introduction

The neutron spin resonance mode is a prominent clue to understand the magnetically driven superconductivity in unconventional superconductors.[1,2] Experimentally, it is a sharp peak emerging in the low-energy spin excitations with intensity behaving like a superconducting order parameter, which has been extensively observed in copper-oxide,[3,4] heavy-fermion,[5,6] iron-pnictide,[7] and iron-chalcogenide superconductors.[8] The resonance energy E_R defined at the peak point is generally proportional to the superconducting transition temperature (T_c) with a universal ratio $E_R/k_BT_c = 4$–6.[1,2,9–12] Theoretically, the neutron spin resonance mode is commonly regarded as a spin exciton arising from the collective particle–hole excitations of gapped Cooper pairs. In this picture, the entire spin resonance should be below a spin-flip continuum energy $\hbar\omega_c$ just beneath the pair-breaking gap 2Δ (Δ is the superconducting gap),[1,2] and usually the mode energy follows another linear scaling $E_R/2\Delta \approx 0.6$ for most of unconventional superconductors.[13,14] When the spin resonance disperses to high energy approaching $\hbar\omega_c$, it will become weaker and weaker, then finally damps out after entering the particle–hole continuum.[1,2] Therefore, the superconducting gap determines not only the upper limit of the resonance energy, but also the shape of the resonance dispersion.[12,15] In cuprates with d-wave pairing, $\hbar\omega_c$ seems like a complete dome with a strong momentum dependence from antinodal ($\Delta_{max} = \Delta_0$) to nodal region ($\Delta_{min} = 0$), resulting in a downward dispersion of spin resonance with $E_R < 2\Delta_0$.[1] In iron-based superconductors, the superconducting pairing symmetry is generally believed as a sign-reversed $s^{\pm}$-wave between the hole and electron Fermi pockets.[16,17] The spin resonance arises from quasiparticle excitations with a finite wavevector $\boldsymbol{Q}$ that connects those sign-changed pairs of Fermi pockets, thus $\hbar\omega_c$ is defined by the total superconducting gap summed on them: $\hbar\omega_c = \Delta_{tot} = |\Delta_k| + |\Delta_{k+Q}|$. Δ_{tot} is momentum independent when only two similar sized Fermi pockets nest with each other.[18–20] In this case, a magnon-like upward dispersion of spin resonance is expected to be beneath the near constant ceiling of Δ_{tot}. This upward dispersion of spin resonance in the superconducting state is closely related to the anisotropic spin–spin correlation length in the normal state, but has a much lower velocity than the antiferromagnetic (AF) spin waves in parent compounds.[21–23] In most cases, the size mismatch of Fermi pockets together with the distribution of multiple gaps may further affect the dispersion of the resonance.[23,24]

*Project supported by the National Key Research and Development Program of China (Grant Nos. 2018YFA0704200, 2018YFA0305602, 2017YFA0303100, and 2017YFA0302900), the National Natural Science Foundation of China (Grant Nos. 11822411 and 11961160699), the Strategic Priority Research Program (B) of the Chinese Academy of Sciences (CAS) (Grant Nos. XDB25000000 and XDB07020300), K.C.Wong Education Foundation (Grant No. GJTD-2020-01), the Youth Innovation Promotion Association of CAS (Grant No. Y202001), and the Beijing Natural Science Foundation, China (Grant No. JQ19002).

†These authors contributed equally.

‡Corresponding author. E-mail: hqluo@iphy.ac.cn

§Present address: Neutron Scattering Division, Oak Ridge National Laboratory, Oak Ridge, Tennessee 37831, USA.

Although the spin resonance mode has been observed in almost all of iron-based superconductors and generally follows both linear relations: $E_R/k_BT_c \approx 4.9$ and $E_R/\Delta_{tot} \approx 0.64$,[11–14] the resonance energy may exceed Δ_{tot} in several particular compounds such as $K_xFe_{2-y}(Se_{1-z}S_z)_2$,[25] $(CaFe_{1-x}Pt_xAs)_{10}Pt_3As_8$,[26] $(Li_{0.8}Fe_{0.2})ODFeSe$[27] and $ACa_2Fe_4As_4F_2$ (A = K, Cs).[12,28] Instead of the excitonic scenario under $s^{\pm}$-pairing, some of them may be alternatively explained as the self-energy effect induced redistribution of spin excitations under sign-preserved (s^{++}) pairing.[29,30] In addition to the mode energy E_R at antiferromagnetic wavevector $\boldsymbol{Q}_{AF}$, the dispersion of the spin resonance seems to highly depend on the magnetic interactions in different compounds.[9] Weak out-of-plane dispersion of the spin resonance mode along L direction has been found in those superconducting compounds proximate to the three-dimensional (3D) stripe-type AF order [e.g., $BaFe_{2-x}(Ni, Co, Ru)_xAs_2$, $BaFe_2(As_{1-x}P_x)_2$, $NaFe_{1-x}Co_xAs$, $Ba_{1-x}Na_xFe_2As_2$, etc.],[31–37] while in those compounds with weak spin–orbital coupling (such as $Ca_{1-y}La_yFe_{1-x}Ni_xAs_2$) or stoichiometric superconductivity (such as $KCa_2Fe_4As_4F_2$), the spin resonance is two-dimensional (2D) in reciprocal space.[11,12] In the bilayer $CaKFe_4As_4$ system, the resonance intensity splits into two opposite harmonic modulations showing odd and even symmetries along L direction with respect to the distance of Fe–Fe planes within the Fe–As bilayer unit, but the resonance energies for both odd and even modes are L independent.[14] So far, the investigations on the in-plane dispersion (along H or K direction) of spin resonance are quite limited in iron-based superconductors, since it is a great challenge to map the weak resonant signals away from the zone center $\boldsymbol{Q}_{AF}$ and peak energy E_R. Previous inelastic neutron scattering measurements on $BaFe_{2-x}Ni_xAs_2$ reveal an upward in-plane dispersion of the resonance mode, thus it supports the spin excitonic picture and also explains the weak L dispersion as a consequence of the residual weak interlayer spin correlations.[21,24] However, an unusual downward in-plane dispersion of the resonance was recently discovered in the quasi-2D $KCa_2Fe_4As_4F_2$, which apparently exceeds Δ_{tot} and deeply challenges the spin excitonic picture.[12] Therefore, it is essential to fully compare the in-plane dispersion of spin resonance mode with the superconducting gaps in each system of iron-based superconductors.

It was noted that the ringlike upward in-plane dispersion of spin resonance in $Ba_{0.67}K_{0.33}(Fe_{1-x}Co_x)_2As_2$ probably arises from particle–hole excitations on the imperfectly nested electron–hole Fermi surfaces.[23] However, their measurements were undertaken by time-of-flight neutron scattering experiments with fixed $k_i \parallel c^*$, which means the energy transfer is always coupled with the momentum transfer along L direction. Previous reports on the band structure and superconducting gaps of $Ba_{1-x}K_xFe_2As_2$ are controversial, thus the random phase approximation (RPA) calculation of the spin exciton model is inadequate to capture the details of the resonance dispersion.[22,23] Here, we measure the in-plane dispersion of spin resonance mode in $Ba_{0.67}K_{0.33}Fe_2As_2$ in fixed L planes in more detail using a triple-axis neutron scattering spectrometer, and compare with the gap distributions recently measured by high resolution angle resolved photoemission spectroscopy (ARPES). Our results show that the spin resonance quickly becomes incommensurate for $E \geqslant 11$ meV and disperses upwards at least up to $E = 26$ meV, much higher than Δ_{tot} for all kinds of combination of hole–electron pockets. Therefore, the dispersion of the spin resonance cannot be fully accounted by particle–hole excitons under $s^{\pm}$-pairing, as it may not be restricted by superconducting gaps in such multiband systems.

2. Experimental setup

High quality single crystals of $Ba_{0.67}K_{0.33}Fe_2As_2$ were grown by self-flux method using FeAs as flux.[38,39] The largest sizes of our crystals are near 20 mm with homogenous composition. For neutron scattering experiments, about 11 g of crystals were co-aligned on rectangular aluminum plates by x-ray Laue camera using CYTOP hydrogen-free glue [Fig. 1(a)]. Resistivity measurements on typical samples show a very sharp superconducting transition at $T_c = 38.2$ K within $\Delta T \approx 1$ K [Fig. 1(b)]. Magnetization measurements also show a sharp superconducting transition and a nearly full diamagnetic susceptibility $4\pi\chi \approx -1$ [Fig. 1(c)]. For easy comparison, we summarized the superconducting gap values measured by ARPES on optimally doped $Ba_{1-x}K_xFe_2As_2$ in Fig. 1(d).[40–46] Since all measurements suggested isotropic (s-wave) gaps on each Fermi pockets at fixed k_z, here Δ_{tot} is the sum of the absolute gap value on a pair of hole–electron pockets connected by momentum transfer $\boldsymbol{Q}$, as shown in the inset of Fig. 1(d), where the deviations from the center point $[Q = (1,0)]$ are due to the mismatch of the connected hole and electron pockets, and the horizontal bars on the data points mark their distribution in the reciprocal space. The early ARPES measurements seemed to overestimate the gap value, giving $\Delta_{tot} = 16$–24 meV [upper arc in Fig. 1(d)].[40–42] From high resolution ARPES measurements based on high quality crystals,[43–45] especially the most recently published results based on laser-ARPES,[46] we estimated $\Delta_{tot} = 11$–17 meV, which forms a lower downward arc shape along the longitudinal direction [Fig. 1(d)]. Neutron scattering experiments were performed using thermal neutron triple-axis spectrometers EIGER at the Swiss Spallation Neutron Source (SINQ), Paul Scherrer Institut, Switzerland, with fixed final energy $E_f = 14.7$ meV.[47] The scattering plane $[H,0,0] \times [0,0,L]$ is defined by a pseudo-orthorhombic magnetic unit cell with $a \approx b \approx 5.52$ Å, $c = 13.22$ Å, and the vector $\boldsymbol{Q}$ in reciprocal space is defined as $\boldsymbol{Q} = H\boldsymbol{a}^* + K\boldsymbol{b}^* + L\boldsymbol{c}^*$, where H, K, and L

are Miller indices and $\boldsymbol{a}^* = \hat{a}2\pi/a, \boldsymbol{b}^* = \hat{b}2\pi/b, \boldsymbol{c}^* = \hat{c}2\pi/c$ are reciprocal lattice basis vectors. In this case, the AF wave vector is $\boldsymbol{Q}_{\rm AF} = [1,0,L]$ ($L = \pm 1, \pm 3, \pm 5$), and $\boldsymbol{q} = \boldsymbol{Q} - \boldsymbol{Q}_{\rm AF}$ is the vector away from the zone center to describe the dispersion. The total sample mosaic, defined by the full-width-at-half-maximum (FWHM) of the rocking curve, was about 2.6° for peak (2, 0, 0) and 2.8° for peak (0, 0, 4). In Fig. 1(e), we schematically depict the low-energy spin waves of the parent compound $BaFe_2As_2$,[48] together with the dispersion of spin resonance in a doped compound. If the spin resonance is indeed from particle–hole excitons under s$^{\pm}$-pairing, it should be entirely below $\Delta_{\rm tot}$ with upward dispersions but much slower velocity than the spin waves in the parent compound.[21–24]

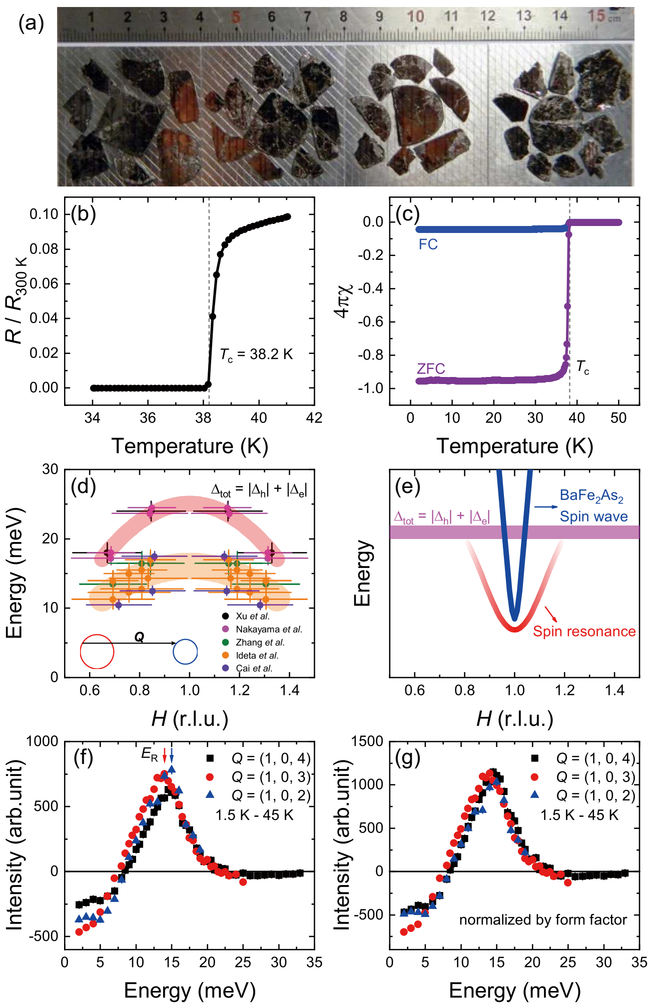

Fig. 1. (a) Photo of $Ba_{0.67}K_{0.33}Fe_2As_2$ crystals used in our neutron scattering experiments. (b) Resistivity transition of superconductivity at $T_c = 38.2$ K. (c) Magnetization transition of superconductivity under field-cooling (FC) and zero-field-cooling (ZFC). (d) The total superconducting gaps $\Delta_{\rm tot} = |\Delta_k| + |\Delta_{k+Q}|$ on the hole and electron Fermi pockets linked by wavevector $\boldsymbol{Q}$ obtained from ARPES results. (e) Comparison between the dispersion of spin resonance mode in the superconducting compound and the spin wave in the parent compound ($BaFe_2As_2$) as predicted by the magnetic exciton scenario under s$^{\pm}$-pairing symmetry, here assuming $\Delta_{\rm tot}$ is momentum independent. (f) The neutron spin resonance peaks at $Q = (1,0,L)$ ($L = 2,3,4$) deduced by subtracting the spin excitations at normal state ($T = 45$ K) from those at superconducting state ($T = 1.5$ K). (g) The neutron spin resonance peaks normalized by the magnetic form factor of Fe^{2+}.

3. Results and discussion

We firstly identify the spin resonance peak by constant-Q scans (energy scans) at $Q = (1,0,L)$ ($L = 2,3,4$). By subtracting the spin excitations at normal state ($T = 45$ K) from those at superconducting state ($T = 1.5$ K), we find a strong peak with clear intensity gain from 8 meV to 20 meV in superconducting state, the peak position for $L = 2$ and 4 is 15 meV, and for $L = 3$ is slightly lower at 14 meV [Fig. 1(f)]. By further normalizing the intensity using the square of magnetic form factor of Fe^{2+} ($|F(Q)|^2$), it seems that all three peaks have similar shape except for a small shift to low energy side for $L = 3$. Such results suggest that the spin resonance intensity does not have any L modulation, and the L dispersion of $E_{\rm R}$ is very weak, namely, the resonance mode is nearly 2D in reciprocal space. These results are consistent with previous reports on the spin resonance energy and the weak k_z modulation in most of superconducting gaps.[23,39,45]

To determine the in-plane dispersion of the spin resonance, we have performed constant-energy scans (Q-scans) along $\boldsymbol{Q} = [H,0,3]$ from $E = 3$ meV to 24 meV both at $T = 1.5$ K (superconducting state) and $T = 45$ K (normal state). Due to the limitation from spectrometer itself and the scattering rule, the scattering triangle cannot be closed for low Q side of $E = 22$ meV and 24 meV with fixed $L = 3$, we thus measured the $E = 26$ meV along $\boldsymbol{Q} = [H,0,4]$. The raw data are shown in Fig. 2, the flat backgrounds are already subtracted. To confirm the 2D behavior, additional scans at $E = 3$ meV, 9 meV and 18 meV were also measured along $\boldsymbol{Q} = [H,0,4]$ (data not shown). The signals at high energy are contaminated by spurious scattering possibly from the phonons of the sample holder or multiple scattering of Bragg peaks, which should be almost temperature independent within the measured range 1.5–45 K but only broaden the peak width. We find clear enhancements of the intensity above $E = 9$ meV at $T = 1.5$ K from the spin resonance. Due to the opening of full superconducting gaps below T_c, the spin excitations at $E = 3$ meV are nearly fully gapped [Fig. 2(a)], and there are still intensity loss and peak sharpening at $T = 1.5$ K for low energies 3–8 meV, which can be explained as a strengthened spin–spin correlation length responding to the superconducting order.[39] From the raw data, we cannot identify any incommensurate spin excitations even in the superconducting state. Thus we have simply performed the single Gaussian fitting for all raw data peaks both at $T = 1.5$ K and $T = 45$ K, as shown by solid lines in Fig. 2. The FWHM of such fitting roughly reflects the energy and temperature dependence of the spin–spin correlation length [Fig. 4(c)].

From those Q-scans in Fig. 2, we obtain clean Q-distribution of the spin resonance by doing subtraction ΔInt. = Int.($T = 1.5$ K) − Int.($T = 45$ K), as shown in Fig. 3. The spin gap at $E = 3$ meV has similar peak width for $L = 3$

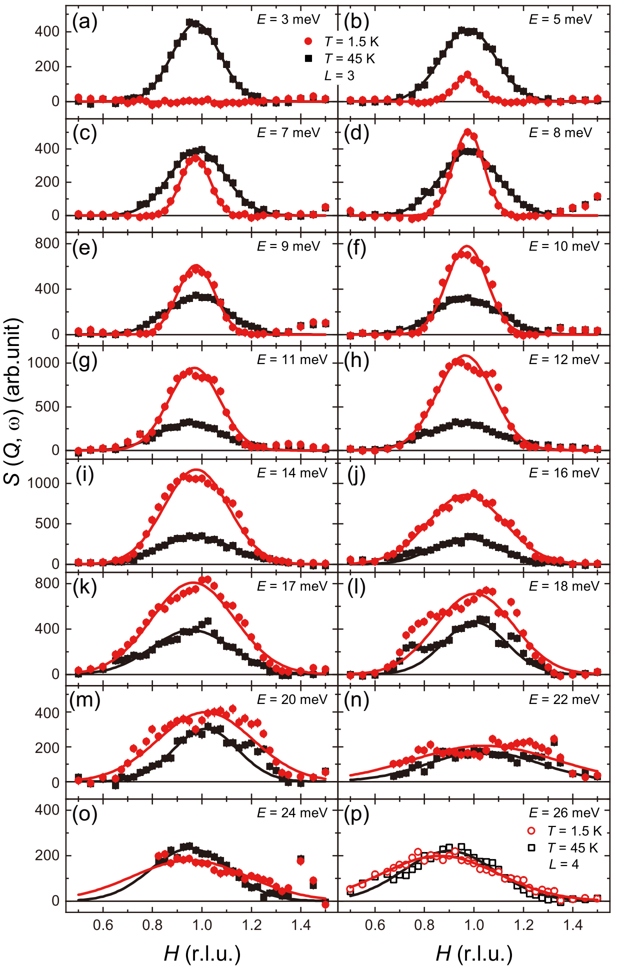

Fig. 2. Constant-energy scans along $\boldsymbol{Q} = [H, 0, 3]$ from $E = 3$ meV to 24 meV and along $\boldsymbol{Q} = [H, 0, 4]$ for $E = 3$ meV , 18 meV and 26 meV measured both at $T = 1.5$ K (red) and $T = 45$ K (black). The solid lines are fitting curves by single Gaussian functions.

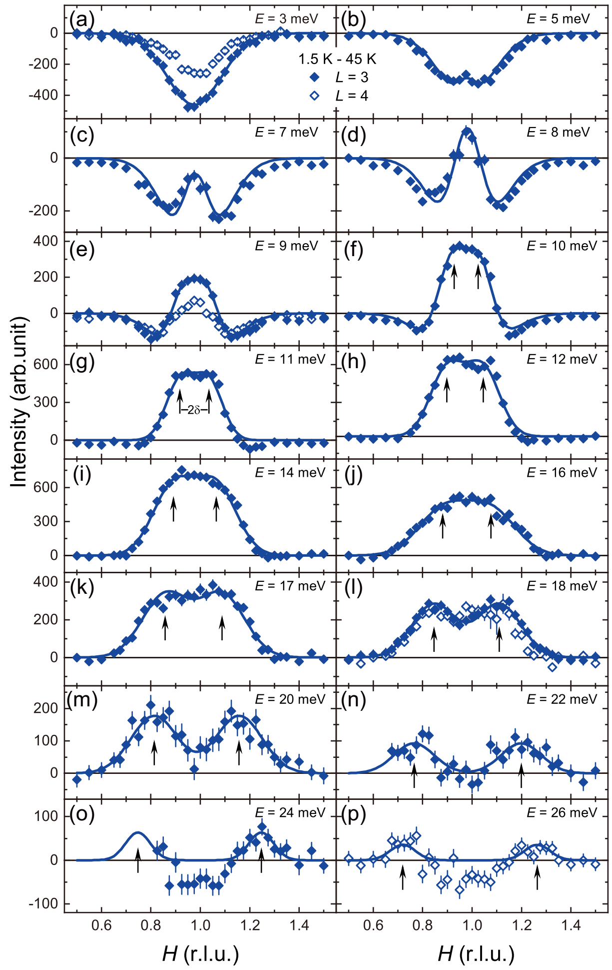

Fig. 3. The difference between $T = 1.5$ K and 45 K of constant-energy scans in Fig. 2 (ΔInt. = Int.($T = 1.5$ K) − Int.($T = 45$ K)). The solid lines for $E = 3$ meV, 5 meV, 7 meV, 8 meV, 9 meV are obtained by the difference (1.5 K − 45 K) of single Gaussian fitting in Fig. 2, and other solid lines for $E = 10$–26 meV are fitting curves by two symmetric Gaussian functions. For comparison, the results along $\boldsymbol{Q} = [H, 0, 4]$ at $E = 3$ meV, 18 meV and 26 meV are also presented by open symbols.

(FWHM = 0.259 r.l.u.) and $L = 4$ (FWHM = 0.245 r.l.u.) [Fig. 3(a)]. At the commensurate position of $Q_{\rm AF} = (1, 0, 3)$ (Brillouin zone center with $q = 0$), the change of correlation length firstly induces a small tip in the center of ΔInt at $E = 5$ meV [Fig. 3(b)], and evolves to two negative peaks at $E = 7$ meV [Fig. 3(c)] and a partially positive peak at $E = 8$ meV [Fig. 3(d)]. To identify the starting energy of resonance intensity, we integrate ΔInt. and then find that it becomes positive when $E > 9$ meV [Fig. 3(e)], as there is certainly a positive peak at $E = 10$ meV [Fig. 3(f)]. Therefore, the spin resonance actually emerges between 9 meV and 10 meV, or even lower energy ~ 8 meV if only considering the excitations near $q = 0$. The resonance peak quickly disperses to incommensurate positions as shown by the data above $E = 11$ meV [Figs. 3(g)–3(p)], because all of them can be well fitted by two symmetric gaussian functions. The incommensurability δ along H does not have L dependence, as manifested by the nearly overlapped data points for $L = 3$ and $L = 4$ at $E = 18$ meV within the experimental errors [Fig. 3(i)]. Thus we could track the in-plane dispersion of spin resonance by combining the results both from $L = 3$ and $L = 4$ due to its 2D nature.

The peak positions determined by the incommensurability are present in Fig. 4(a). For $E = 9$ meV, we simply show the commensurate position with a horizontal error bar to represent the estimated peak width of the positive part. The lower arc shape of $\Delta_{\rm tot}$ from high resolution ARPES measurements shown in Fig. 1(d) is also present in Fig. 4(a) for direct comparison, and the gradient colors represent the intensity of ΔInt. obtained from Fig. 3. Apparently, $\Delta_{\rm tot}$ just cuts through the waist of the resonance mode. Although the most intensity of ΔInt. locates below $E = 17$ meV, the dispersion of the resonance mode can break though $\Delta_{\rm tot}$ and persist to at least $E = 26$ meV [Figs. 3(p) and 4(a)]. We replot the resonance peak in Fig. 4(b) by using the integrated intensity of ΔInt. from constant-energy scans along $\boldsymbol{Q} = [H, 0, 3]$ in Fig. 3. The peak energy still locates at $E = 14$ meV, but the peak shape slightly shifts to high energy in comparison to the E-scan at $Q = (1, 0, 3)$ shown in Fig. 1(f). The peak widths from single Gaussian fitting in Fig. 2 are plotted in Fig. 4(c), both results at $T = 1.5$ K and $T = 45$ K linearly increase upon energy, but the two lines cross around the resonance energy

$E_R = 14$ meV. Namely, the correlation length in superconducting state is elongated below the mode center energy E_R, but shorten above E_R due to the effect from dispersion of the resonance.

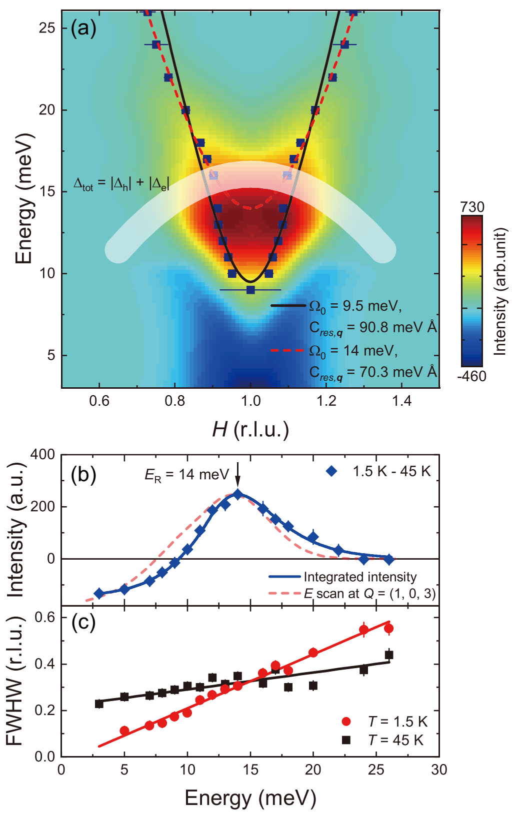

Fig. 4. (a) Dispersion along H of the spin resonance. Here the solid squares mark the incommensurate peak positions from two-Gaussian-fitting of the resonance peaks, the horizontal bar at $E = 9$ meV is the estimated width for positive part of ΔInt., and the contour colors represent the intensity obtained from the solid lines in Fig. 3. The distribution of Δ_{tot} is also shown as the white arc [same as the lower arc in Fig. 1(d)]. (b) Integrated intensity of ΔInt. obtained from constant-energy scans along $\boldsymbol{Q} = [H, 0, 3]$ in Fig. 3. The solid line is guide to eyes, and the dashed line is normalized intensity from the E-scan at $Q = (H, 0, 3)$ in Fig. 1(f). (c) Comparison of the peak width between $T = 1.5$ K and $T = 45$ K along $\boldsymbol{Q} = [H, 0, 3]$ from single-Gaussian-fitting curves in Fig. 2.

In the spin exciton model, the spin resonance is a bound state inside the superconducting state formed by electron–hole (singlet-triplet) excitations. Such exciton is a consequence of spin interactions already present in the normal state when the superconducting gaps open below T_c.[1,2] Under the commonly believed $s^{\pm}$-pairing symmetry in iron-based superconductors, the dispersion of spin resonance is in the form of a gapped magnon with upward dispersion: $\Omega_{\boldsymbol{q}} = \sqrt{\Omega_0 + c^2_{\text{res},\boldsymbol{q}} q^2}$, where Ω_0 is the resonance energy at zone center Q_{AF} ($\boldsymbol{q} = 0$), and the spin velocity $c_{\text{res},\boldsymbol{q}} = \Omega_0 \xi_{\boldsymbol{q}}$ is related to the normal state spin–spin correlation length $\xi_{\boldsymbol{q}}$ (assuming the Landau damping is isotropic).[21,23] From previous time-of-flight neutron scattering experiments, we can extract $\xi_{\boldsymbol{q}} \approx 10.8$ Å for $Ba_{0.67}K_{0.33}Fe_2As_2$.[23,49] If we assume the resonance mode starting from $E_R = 14$ meV with the strongest intensity, then $\Omega_0 = E_R = 14$ meV will give $c^{\text{cal}}_{\text{res},\boldsymbol{q}} = 151.2$ meV·Å from calculation, but fitting by the above equation will yield $c^{\text{exp}}_{\text{res},\boldsymbol{q}} = 70.3$ meV·Å (red dashed line in Fig. 4(a)). In fact, from the data shown in Fig. 3, we believe that the spin resonance should start between $E = 9$ meV and $E = 10$ meV, since it already disperses to incommensurate positions above 11 meV. Thus it is more reasonable to take $\Omega_0 = 9.5$ meV, giving $c^{\text{cal}}_{\text{res},\boldsymbol{q}} = 102.6$ meV·Å from calculation and $c^{\text{exp}}_{\text{res},\boldsymbol{q}} = 90.8$ meV·Å from fitting (black solid line in Fig. 4(a)). Apparently, the latter estimation seems to be more consistent with each other, but it still can not explain why the resonance survives away above Δ_{tot}. Interestingly, the resonance disperison in Fig. 4(a) shows a clear kink around Δ_{tot}, suggesting different spin velocity below and above Δ_{tot}. Thus it is possible that the resonance may have different origins for energy range below and above Δ_{tot}. For example, excitonic excitations under $s^{\pm}$-pairing play a key role for the spin resonance at the low-energy range, which requires all of them below Δ_{tot} with much slower spin velocity in the superconducting state.[20–23,51–53] Above Δ_{tot}, the self-energy effect under s^{++}-pairing may dominate at the high-energy range as predicted by the RPA calculations[20–22,29,30,54,55] and also shown in $K_xFe_{2-y}(Se_{1-z}S_z)_2$ system.[25] However, the self-energy effect induced redistribution of spin excitations in s^{++} superconducting state would basically follow the spin excitation dispersion at normal state,[20,22,29,30,54,55] which has a very large velocity similar to the spin waves in parent compound $c_{\text{nor},\boldsymbol{q}} \approx 450$ meV·Å.[9,21,23,49] It should be noticed that the iron-based superconductors are multi-band systems with different superconducting gaps on each band, so the scattering from Γ to M points has many channels under different energy limits,[16,17] which can result in multiple spin resonance modes. If $\Delta_{\text{tot,q}}$ on each pair of bands are similar, then the spin resonance mode is highly degenerated. In this sense, it is impossible to analyze the dispersion of the resonance by treating it as a single mode. It is worth to notice that the nondegenerate spin resonance including odd and even modes at quite different energies in $CaKFe_4As_4$ may provide an excellent chance to clarify this issue.[14,50] Further analysis is necessary to identify the contribution of each band or each orbital in the spin resonance mode.

4. Conclusion

To summarize, we have carefully examined the in-plane dispersion of spin resonance mode in $Ba_{0.67}K_{0.33}Fe_2As_2$. The mode energy with maximum intensity locates at $E = 14$ meV for $Q = (1, 0, 3)$, but the resonance may emerge at lower energy ($E = 9$–10 meV) and quickly disperse to incommensurate positions ($q \neq 0$) persisting up to $E = 26$ meV. While the estimated resonance velocity by the spin exciton model agrees reasonably well with experimental observation, the dispersion of spin resonance breaks through the limit of the total superconducting gaps Δ_{tot}. Our results suggest that the detailed behaviors of spin resonance in iron-based superconductors may be closely related to its multi-band nature. By comparing them among different systems would inspire new mechanisms of magnetically driven superconductivity.

Acknowledgments

The authors thanks the helpful discussion with Prof. Jiangping Hu and Prof. Jianxin Li. This work is based on neutron scattering experiments performed at the Swiss Spallation Neutron Source (SINQ), Paul Scherrer Institut, Villigen, Switzerland (Proposal No. 20180227).

References

[1] Eschrig M 2006 *Adv. Phys.* **55** 47
[2] Sidis Y, Pailhès S, Hinkov V, Fauqué B, Ulrich C, Capogna L, Ivanov A, Regnault L P, Keimer B and Bourges P 2007 *C. R. Phys.* **8** 745
[3] Rossat-Mignod J, Regnault L P, Vettier C, Bourges P, Burlet P, Bossy J, Henry J Y and Lapertot G 1991 *Physica C* **185–189** 86
[4] Mook H A, Yethiraj M, Aeppli G, Mason T E and Armstrong T 1993 *Phys. Rev. Lett.* **70** 3490
[5] Sato N K, Aso N, Miyake K, Shiina R, Thalmeier P, Varelogiannis G, Geibel C, Steglich F, Fulde P and Komatsubara T 2001 *Nature* **410** 340
[6] Stock C, Broholm C, Hudis J, Kang H J and Petrovic C 2008 *Phys. Rev. Lett.* **100** 087001
[7] Christianson A D, Goremychkin E A, Osborn R, Rosenkranz S, Lumsden M D, Malliakas C D, Todorov I S, Claus H, Chung D Y, Kanatzidis M G, Bewley R I and Guidi T 2008 *Nature* **456** 930
[8] Liu T J, Hu J, Qian B, Fobes D, Mao Z Q, Bao W, Reehuis M, Kimber S A J, Prokes K, Matas S, Argyriou D N, Hiess A, Rotaru A, Pham H, Spinu L, Qiu Y, Thampy V, Savici A T, Rodriguez J A and Broholm C 2010 *Nat. Mater.* **9** 716
[9] Dai P 2015 *Rev. Mod. Phys.* **87** 855
[10] Wang M, Luo H, Zhao J, Zhang C, Wang M, Marty K, Chi S, Lynn J W, Schneidewind A, Li S and Dai P 2010 *Phys. Rev. B* **81** 174524
[11] Xie T, Gong D, Ghosh H, Ghosh A, Soda M, Masuda T, Itoh S, Bourdarot F, Regnault L P, Danilkin S, Li S and Luo H 2018 *Phys. Rev. Lett.* **120** 137001
[12] Hong W, Song L, Liu B, Li Z, Zeng Z, Li Y, Wu D, Sui Q, Xie T, Danilkin S, Ghosh H, Ghosh A, Hu J, Zhao L, Zhou X, Qiu X, Li S and Luo H 2020 *Phys. Rev. Lett.* **125** 117002
[13] Yu G, Li Y, Motoyama E M and Greven M 2009 *Nat. Phys.* **5** 873
[14] Xie T, Wei Y, Gong D, Fennell T, Stuhr U, Kajimoto R, Ikeuchi K, Li S, Hu J and Luo H 2018 *Phys. Rev. Lett.* **120** 267003
[15] Song Y, Van Dyke J, Lum I K, White B D, Jang S, Yazici D, Shu L, Schneidewind A, Čermák P, Qiu Y, Maple M B, Morr D K and Dai P 2016 *Nat. Commun.* **7** 12774
[16] Richard P, Sato T, Nakayama K, Takahashi T and Ding H 2011 *Rep. Prog. Phys.* **74** 124512
[17] Hirschfeld P J, Korshunov M M and Mazin I I 2011 *Rep. Prog. Phys.* **74** 124508
[18] Maier T A and Scalapino D J 2008 *Phys. Rev. B* **78** 020514(R)
[19] Maier T A, Graser S, Scalapino D J and Hirschfeld P 2009 *Phys. Rev. B* **79** 134520
[20] Das T and Balatsky A V 2011 *Phys. Rev. Lett.* **106** 157004
[21] Kim M G, Tucker G S, Pratt D K, Ran S, Thaler A, Christianson A D, Marty K, Calder S, Podlesnyak A, Bud'ko S L, Canfield P C, Kreyssig A, Goldman A I and McQueeney R J 2013 *Phys. Rev. Lett.* **110** 177002
[22] Zhang C, Li H F, Song Y, Su Y, Tan G, Netherton T, Redding C, Carr S V, Sobolev O, Schneidewind A, Faulhaber E, Harriger L W, Li S, Lu X, Yao D X, Das T, Balatsky A V, Brückel Th, Lynn J W and Dai P 2013 *Phys. Rev. B* **88** 064504
[23] Zhang R, Wang W, Maier T A, Wang M, Stone M B, Chi S, Winn B and Dai P 2018 *Phys. Rev. B* **98** 060502(R)
[24] Luo H, Lu X, Zhang R, Wang M, Goremychkin E A, Adroja D T, Danilkin S, Deng G, Yamani Z and Dai P 2013 *Phys. Rev. B.* **88** 144516
[25] Wang Q, Park J T, Feng Y, Shen Y, Hao Y, Pan B, Lynn J W, Ivanov A, Chi S, Matsuda M, Cao H, Birgeneau R J, Efremov D V and Zhao J 2016 *Phys. Rev. Lett.* **116** 197004
[26] Surmach M A, Brückner F, Kamusella S, Sarkar R, Portnichenko P Y, Park J T, Ghambashidze G, Luetkens H, Biswas P K, Choi W J, Seo Y I, Kwon Y S, Klauss H H and Inosov D S 2015 *Phys. Rev. B* **91** 104515
[27] Ma M, Wang L, Bourges P, Sidis Y, Danilkin S and Li Y 2017 *Phys. Rev. B* **95** 100504
[28] Adroja D T, Blundell S J, Lang F, Luo H, Wang Z and Cao G 2020 *J. Phys.: Condens. Matter* **32** 435603
[29] Kontani H and Onari S 2010 *Phys. Rev. Lett.* **104** 157001
[30] Takeuchi L, Yamakawa Y and Kontani H 2018 *Phys. Rev. B* **98** 165143
[31] Chi S, Schneidewind A, Zhao J, Harriger L W, Li L, Luo Y, Cao G, Xu Z, Loewenhaupt M, Hu J and Dai P 2009 *Phys. Rev. Lett.* **102** 107006
[32] Wang M, Luo H, Zhao J, Zhang C, Wang M, Marty K, Chi S, Lynn J W, Schneidewind A, Li S and Dai P 2010 *Phys. Rev. B* **81** 174524
[33] Park J T, Friemel G, Li Y, Kim J H, Tsurkan V, Deisenhofer J, Krug von Nidda H A, Loidl A, Ivanov A, Keimer B and Inosov D S 2011 *Phys. Rev. Lett.* **107** 177005
[34] Zhao J, Rotundu C R, Marty K, Matsuda M, Zhao Y, Setty C, Bourret-Courchesne E, Hu J and Birgeneau R J 2013 *Phys. Rev. Lett.* **110** 147003
[35] Lee C H, Steffens P, Qureshi N, Nakajima M, Kihou K, Iyo A, Eisaki H and Braden M 2013 *Phys. Rev. Lett.* **111** 167002
[36] Zhang C, Yu R, Su Y, Song Y, Wang M, Tan G, Egami T, Fernandez-Baca J A, Faulhaber E, Si Q and Dai P 2013 *Phys. Rev. Lett.* **111** 207002
[37] Waßer F, Park J T, Aswartham S, Wurmehl S, Sidis Y, Steffens P, Schmalzl K, Büchner B and Braden M 2019 *npj Quantum Mater.* **4** 59
[38] Luo H, Wang Z, Yang H, Cheng P, Zu X and Wen H H 2008 *Supercond. Sci. Technol.* **21** 125014
[39] Zhang C, Wang M, Luo H, Wang M, Liu M, Zhao J, Abernathy D L, Maier T A, Marty K, Lumsden M D, Chi S, Chang S, Rodriguez-Rivera J A, Lynn J W, Xiang T, Hu J and Dai P 2011 *Sci. Rep.* **1** 115
[40] Ding H, Richard P, Nakayama K, Sugawara K, Arakane T, Sekiba Y, Takayama A, Souma S, Sato T, Takahashi T, Wang Z, Dai X, Fang Z, Chen G, Luo J and Wang N 2008 *Europhys. Lett.* **83** 47001
[41] Nakayama K, Sato T, Richard P, Xu Y M, Sekiba Y, Souma S, Chen G, Luo J, Wang N, Ding H and Takahash T 2009 *Europhys. Lett.* **85** 67002
[42] Xu Y M, Huang Y B, Cui X Y, Razzoli E, Radovic M, Shi M, Chen G F, Zheng P, Wang N L, Zhang C L, Dai P C, Hu J P, Wang Z and Ding H 2011 *Nat. Phys.* **7** 198
[43] Zhang Y, Yang L X, Chen F, Zhou B, Wang X F, Chen X H, Arita M, Shimada K, Namatame H, Taniguchi M, Hu J P, Xie B P and Feng D L 2010 *Phys. Rev. Lett.* **105** 117003
[44] Zhang Y, Ye Z R, Ge Q Q, Chen F, Jiang J, Xu M, Xie B P and Feng D L 2012 *Nat. Phys.* **8** 371
[45] Ideta S, Murai N, Nakajima M, Kajimoto R and Tanaka K 2019 *Phys. Rev. B* **100** 235135
[46] Cai Y, Huang J, Miao T, Wu D, Gao Q, Li C, Xu Y, Jia J, Wang Q, Huang Y, Liu G, Zhang F, Zhang S, Yang F, Wang Z, Peng Q, Xu Z, Zhao L and Zhou X J 2021 *Science Bulletin* **66** 1839
[47] Stuhr U, Roessli B, Gvasaliya S, Rønnow H M, Filges U, Graf D, Bollhalder A, Hohl D, Bürge R, Schild M, Holitzner L, Kaegi C, Keller P and Mühlebach T 2017 *Nucl. Instrum. Methods Phys. Res., Sect. A* **853** 16
[48] Harriger L W, Luo H, Liu M, Frost C, Hu J, Norman M R and Dai P 2011 *Phys. Rev. B* **84** 054544
[49] Wang M, Zhang C, Lu X, Tan G, Luo H, Song Y, Wang M, Zhang X, Goremychkin E A, Perring T G, Maier T A, Yin Z, Haule K, Kotliar G and Dai P 2013 *Nat. Commun.* **4** 2874
[50] Xie T, Liu C, Bourdarot F, Regnault L P, Li S and Luo H 2020 *Phys. Rev. Research* **2** 022018(R)
[51] Qiu Y, Bao W, Zhao Y, Broholm C, Stanev V, Tesanovic Z, Gasparovic Y C, Chang S, Hu J, Qian B, Fang M and Mao Z 2009 *Phys. Rev. Lett.* **103** 067008
[52] Inosov D S, Park J T, Bourges P, Sun D L, Sidis Y, Schneidewind A, Hradil K, Haug D, Lin C T, Keimer B and Hinkov V 2010 *Nat. Phys.* **6** 178
[53] Korshunov M M and Eremin I 2008 *Phys. Rev. B* **78** 140509
[54] Onari S, Kontani H and Sato M 2010 *Phys. Rev. B* **81** 060504
[55] Onari S and Kontani H 2011 *Phys. Rev. B* **84** 144518